ISSN 0036-0236, Russian Journal of Inorganic Chemistry, 2009, Vol. 54, No. 14, pp. 2091–2106. © Pleiades Publishing, Ltd., 2009.

Mesostructure, Fractal Properties and Thermal Decomposition of Hydrous Zirconia and Hafnia[1]

V. K. Ivanov[a], G. P. Kopitsa[b], A. Ye. Baranchikov[a], M. Sharp[c], K. Pranzas[c], and S. V. Grigoriev[b]

[a]*Kurnakov Institute of General and Inorganic Chemistry, Moscow 119991, Russia*

[b]*Petersburg Nuclear Physics Institute, Russian Academy of Sciences, Gatchina, 188300 Russia*

[c]*GKSS Research Centre, D-21502 Geesthacht, Germany*

Received May 15, 2009

Abstract—By use of small angle and ultra small angle neutron scattering techniques it was established that amorphous xerogels of hydrous zirconia and hafnia possess fractal properties in a wide range of scales, and the fractal dimension of these materials can be intentionally modified by changing their precipitation pH. It was found that the changes in fractal dimension and specific surface area of hydrous zirconia and hafnia xerogels are governed by the changes in the adsorption of anions onto their surface. It was demonstrated that particle size and specific surface area of ZrO_2 and HfO_2 nanopowders prepared by thermal decomposition of hydrous zirconia and hafnia xerogels depends strongly on the mesostructure and synthesis conditions of these xerogels.

DOI: 10.1134/S0036023609140022

I. INTRODUCTION

Zirconium and hafnium dioxides (ZrO_2, HfO_2) have many industrial applications due to their unique physico-chemical properties. For instance, zirconia is one of the key components of sensors, catalysts and catalyst supports, membranes, solid electrolytes in solid oxide fuel cells etc. [1–5]. Majority of methods of micro- and nanocrystalline zirconia and hafnia synthesis are based on hydrolysis of zirconium- and hafnium-containing compounds (usually soluble salts of corresponding metals) and subsequent thermal treatment of hydrous precipitates. It was shown that micromorphology of thus obtained powders is strongly influenced by conditions of hydrolysis and further calcination. Moreover, even the phase composition of thus produced zirconium dioxide, namely the content of metastable tetragonal zirconia and stable monoclinic zirconia, is governed by all the interdependent processes taking place during formation of hydrous zirconia and its further dehydration.

The major difficulties arising in study of the influence of synthetic conditions on the micromorphology and structure-sensitive properties of zirconia and hafnia originate first of all from the fact that corresponding hydrous oxides are amorphous or semi-crystalline materials so they cannot be analyzed using traditional methods, namely, X-ray diffraction, electron microscopy etc. This problem can be partially solved by the use of small angle X-ray and neutron scattering. Previously such an approach was successfully used in study of similar objects, especially hydrous amorphous silica [6, 7].

Surprisingly, information on the mesostructure of hydrous zirconia and hafnia is still rather poor. Singhal *et al.* [8] have studied the structure formation of hydrous zirconia polymers in aqueous solutions using small angle X-ray scattering (SAXS) technique. It was found that zirconia primary particles are formed at very low pH values (viz. 1.2). On ageing colloid solutions these particles form large mass fractal aggregates that can further restructure into dense particles. Stachs *et al.* [9] have shown that amorphous zirconia gels prepared by hydrolysis of zirconium propoxide also possess fractal properties which are lost during the process of drying. Zeng *et al.* [10], Lecomte *et al.* [11], Liang *et al.* [12] have studied the fractal characteristics of aerogels produced by supercritical drying of hydrous zirconia gels. It was established that the structure of thus prepared materials is made of interconnected fractal clusters formed by aggregation of small primary particles. According to SAXS data [10–12], the size of monomers and the fractal dimension of their aggregates depend strongly on conditions of hydrolysis and supercritical treatment. Analysis of the evolution of aerogel structure upon calcination was also performed [12]. It was established that SAXS results are in good agreement with the predictions of Cahn's theory for spinodal decomposition. One should note the same behavior was also observed for other gels, namely SnO_2 xerogels [13].

Silva *et al.* [14] have concluded that fractal structure of zirconia gels is destroyed by conventional drying and is preserved in aerogels. On the contrary, it was experimentally shown that zirconia xerogels obtained in this way may possess fractal properties [15]. To resume, peculiarities of ZrO_2 and HfO_2 fractal structure formation, especially in xerogels, are poorly understood.

[1] The article is published in the original.

Thus the aim of the present work was to review the influence of conditions of hydrous zirconia and hafnia xerogels synthesis on their composition and mesostructure as well as thermal properties of these materials. The study was performed using both small angle and ultra small angle neutron scattering (SANS and USANS) in combination with several other methods including electron microscopy, X-ray diffraction, thermal analysis and low temperature nitrogen adsorption.

II. SYNTHESIS AND STRUCTURE OF HYDROUS ZIRCONIA AND HAFNIA

All raw materials used in the experiments were of analytical grade. Zirconium oxynitrate hydrate ($ZrO(NO_3)_2 \cdot xH_2O$, 99% Aldrich) and hafnium tetrachloride ($HfCl_4$, 98%, Aldrich) were separately dissolved in distilled water so that the final concentration of zirconium and hafnium was 0.25 M. To obtain hydrous zirconia and hafnia gels, aqueous ammonia (2.7 M) was added dropwise to corresponding solutions under vigorous stirring until pH reached the desired value. Zirconia hydrogels were synthesized at pH 2.95, 4.03, 5.04, 5.96, 7.09, 7.50, 8.00 or 8.95. Hafnia hydrogels were synthesized at pH 2.98, 4.01, 6.02, 6.98, 8.05 or 9.01. The resultant white precipitates were centrifuged (8000 min^{-1}) and washed repeatedly with distilled water. All hydrogels were further dried in the oven under air flow at 60°C overnight and carefully grounded in agate mortar. For the sake of clarity, the as-synthesized zirconia xerogels were named hereafter Zr-N3, Zr-N4, Zr-N5, Zr-N6, Zr-N7, Zr-N7.5, Zr-N8 and Zr-N9. Hafnia xerogels were named hereafter Hf-N3, Hf-N4, Hf-N6, Hf-N7, Hf-N8 and Hf-N9.

To study the influence of precipitation conditions on the subsequent thermal decomposition of xerogels, small portions of hydrous zirconia xerogels were annealed at 270, 380, 500 and 600°C for 5 h in muffle furnace. Similarly, thermal decomposition of hydrous hafnia was performed at 500, 600 and 700°C for 5 h. All the samples were heated to corresponding temperatures at the rate of 10°C/min and after the annealing they were cooled down to ambient temperature within the furnace. Resulting zirconia powders were named Zr-N3–TTT, Zr-N6–TTT, Zr-N7–TTT and Zr-N9–TTT (here TTT is equal to the temperature of thermal treatment), and hafnia powders were named Hf-N4–TTT, Hf-N6–TTT, Hf-N7–TTT and Hf-N8–TTT. For example, zirconia sample, synthesized at pH 7 and annealed at 500°C was named Zr-N7-500.

X-ray powder diffractograms (XRD) were obtained on Rigaku D/MAX 2500 diffractometer (CuK_α radiation) over a 2θ range of 15°–80° with an increment 0.02°/step. Analysis of XRD patterns of zirconia samples allows to conclude that initial xerogels as well as xerogels, annealed at 270°C are completely amorphous giving two extremely broad peaks (halo) at ~30° and ~50°–60° 2θ. Diffraction pattern of sample Zr-N3 prepared at the lowest pH includes sharp peaks which can be attributed to orthorhombic ammonium nitrate [JCPDS PDF 47-866].

Basing on short-range structural model proposed by Southon *et al.* [16], reproducible extremely broadened peaks on diffractograms of hydrous zirconia xerogels can be caused by X-ray scattering resulting in characteristic patterns, based on average interatomic distances. According to Raman spectroscopy data [16], in short range ordered zirconium hydroxide polymers consisting of cyclic tetramer species Zr-Zr and Zr-O(H) distances (3.539 and 2.106 Å, respectively) are quite close to the observed peaks. Amorphous nature of hydrous zirconia xerogels is also confirmed by TEM and SAED patterns of the samples.

These data are in a good agreement with results presented by Moroz *et al.* [17–19]. In particular, it was established [17] that hydrous zirconia samples precipitated at pH 7 and pH 9 are X-ray amorphous. These precipitates possess short-range ordering similar to the structure of a cubic ZrO_2 phase [18]. A special feature of hydrous zirconia is that the closest Zr–Zr distances in amorphous xerogel are shortened by 0.2 Å in comparison with the cubic ZrO_2 phase, and NO_3– and OH– groups are the constituents of an anionic sublattice [19].

Crystallization of ammonium nitrate in Zr-N3 sample prepared at the lowest pH and the absence of this phase in the samples precipitated at higher pH values is an unexpected yet explainable result. It is well known that hydrous oxides generally have extremely high sorption capacity. Below so called point of zero charge (pH_{pzc}) their surface is positively charged and this charge can be compensated by preferential adsorption of negatively charged ions. Thus sedimentation of hydrous zirconia from zirconyl nitrate solutions under strongly acidic conditions is accompanied by considerable adsorption of NO_3^- ions and NH_4^+ counter-ions which are present in the mother liquor. Our data indicate that these species cannot be removed completely even by repeated washing and upon mild drying they can form a separate crystalline ammonium nitrate phase.

Upon the raise of pH up to the point close to pH_{pzc} the surface of zirconia bears a net zero charge so the amount of adsorbed ions is significantly reduced. The value of pH_{pzc} depends strongly on the composition and particle size as well as composition and ionic strength of electrolyte etc. [20, 21]. Despite the fact that precise value of the point of zero charge of hydrous zirconia was not determined directly in this study, it was reported to be ~6.0–6.7 [22]. We can also confirm the position of point of zero charge at pH ≈ 6 by observed increase of viscosity of gel under these conditions, because such an effect is known to take place upon approaching the point of zero charge of colloid solutions and suspensions [23, 24].

It should be noted that appearance of powders precipitated at different pH could be an accessory confir-

mation of the position of point of zero charge. The starting pH of zirconyl nitrate acidified solution was around 0.5. Upon addition of aqueous ammonia, pH of the solution gradually increases, and at pH ≈ 1 the solution becomes cloudy. Formation of large quantities of white precipitate takes place at pH ≈ 3, while above this point the appearance of the suspensions doesn't change. However, it should be noted that upon centrifugation and washing there is notable difference between products prepared at pH 3, 4, 5, 7, 7.5, 8, 9, on one hand, and precipitate obtained at pH 6, on the other hand. Samples assigned to the first group consist of individual particles that form flat layer when placed on Petri dish, while the sample precipitated at pH 6 looks like a viscous gel. The same behavior was observed also for hydrous hafnia gels. Dehydration of all the samples at 60°C results in formation of semi-transparent monoliths.

Thus we can suggest that disappearance of traces of ammonium nitrate phase upon increasing pH is caused by the lack of electrostatic attraction, so adsorbed ions can be easily removed by repetitive washing. It should be also noted at higher pH values the surface of hydrous zirconia should be negatively charged and so the adsorption of positively charged ammonium ions could take place. Despite of this hydrous zirconia precipitated under alkaline conditions do not contain notable traces of ammonium nitrate. This fact is probably due to weaker adsorption of ammonium ions onto hydrous zirconia surface in comparison with nitrate ions. This supposition is proved indirectly by the Raman spectroscopy data [16], indicating that zirconium hydroxide gels can contain up to ~0.5 nitrate groups per zirconium which are directly bidentate-coordinated to zirconium atoms. Obviously, such a coordination of nitrate groups is the reason of their stronger adsorption.

It should also be noted that the ammonium nitrate mean crystallite size estimated using Scherrer equation (11) is more than 100 nm, so the presence of this phase doesn't have direct influence on SANS curves.

To study the influence of precipitation conditions on the mesostructure of amorphous zirconia and hafnia xerogels SANS technique was used. SANS measurements were performed on SANS-2 setup (FRG1 neutron reactor, GKSS Research Centre, Geesthacht, Germany), which operates in geometry close to a point geometry. The experiments were performed at neutron wavelengths $\lambda = 5.8$ and 11.6 Å with $\Delta\lambda/\lambda = 10\%$ and for four sample-detector distances SD = 1, 3, 9 and 20.7 m, which allowed to perform the measurements of the neutron scattering intensity for momentum transfers in the range $2 \times 10^{-3} < q < 0.25$ Å^{-1} (here: $q = 4\pi\lambda^{-1}\sin(\theta/2)$, θ is the scattering angle). The scattered neutrons were detected by a two-dimensional position-sensitive ^{3}He detector.

The samples of amorphous xerogels of hydrous ZrO_2 and HfO_2 were placed in a 1 mm thick quartz cell. The initial spectra for each q range were corrected using the standard procedure [25] taking into account the scattering from the setup equipment and cell, as well as background. Resulting 2D isotropic spectra were averaged azimuthally and their absolute values were determined by normalizing to the incoherent scattering cross section from vanadium with inclusion of the detector efficiency and apparent density ρ_H for each sample. All measurements were done at room temperature.

The SANS intensity analyzed hereafter was defined as

$$I_s(q) = I(q) - TI_0(q), \quad (1)$$

where $I(q)$ and $I_0(q)$ are the momentum-transfer distribution of the scattering neutrons behind the sample and beam without the sample, respectively, and $T = I/I_0 = \exp(-\Sigma L)$ is the transmission coefficient of the neutrons passing through the sample, where Σ is the integral scattering cross section and L is the sample thickness. The setup resolution function was approximated by a Gaussian and was calculated separately for each distance SD with the use of the standard procedure [26].

Additional information on the structure of hydrous zirconia and hafnia xerogels in the range 100 nm–10 μm was obtained by use of USANS.

The USANS measurements were performed using double crystal diffractometer (DCD) at FRG1 reactor of GKSS Research Center at the neutron wavelength $\lambda = 4.43$ Å with $\Delta\lambda/\lambda = 1 \times 10^{-5}$ [27]. The instrument was equipped with double monochromator unit based on perfect silicon crystals cut along the (111) plane. The first crystal was used to form the neutron beam and the second crystal performed the monochromator function. The angular distribution of neutrons in the beam past the sample (situated behind the double monochromator) was measured by rotating an analyzer crystal (identical to the monochromator crystal) at a minimum angular step of 2×10^{-7} deg. The full width at half height (FWHM) of the instrument line was $w_0 = 2.6 \times 10^{-5}$ Å^{-1}. The momentum transfer was varied within $2 \times 10^{-5} < q < 1 \times 10^{-3}$ Å^{-1}.

Figures 1 and 2 show the experimental curves of differential macroscopic cross section $d\Sigma(q)/d\Omega$ for small angle neutron scattering (after subtracting the background incoherent scattering on hydrogen atoms) for amorphous xerogels of hydrous zirconia (samples Zr-N3, Zr-N5, Zr-N7 and Zr-N9) and hafnia (samples Hf-N4, Hf-N6, Hf-N8 and Hf-N9). The same curves were also obtained for zirconia and hafnia samples precipitated at other pH values. It can be seen that an increase in the precipitation pH results in a clear increase in the SANS intensity, indicating a decrease in the homogeneity of these xerogels in the nuclear density in the range 10–1000 Å.

In SANS experiments, the power-law momentum-transfer dependence of the scattering intensity is usually observed in the form $I(q) \sim q^{-n}$ ($n \le 6$) in a certain momentum-transfer region $q > 1/R$, where R is the characteristic scale of the scattering system. The fractal dimension of the system and the correlation function of

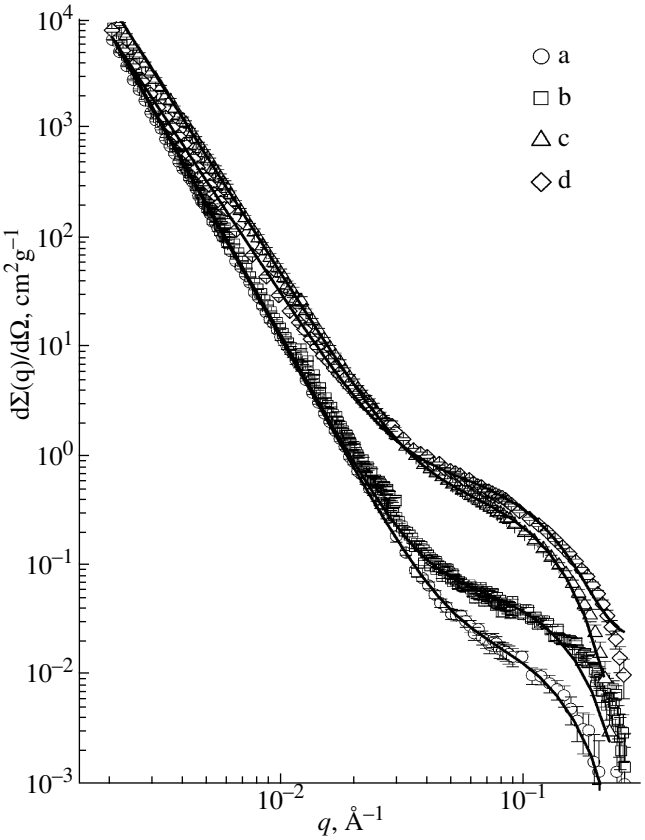

Fig. 1. SANS cross-sections $d\Sigma(q)/d\Omega$ for amorphous $ZrO_2 \cdot xH_2O$ xerogels precipitated at pH 3 (a), 5 (b), 7 (c), and 9 (d) vs. momentum transfer q. Continuous lines represent results of experimental data fitting by equation (3).

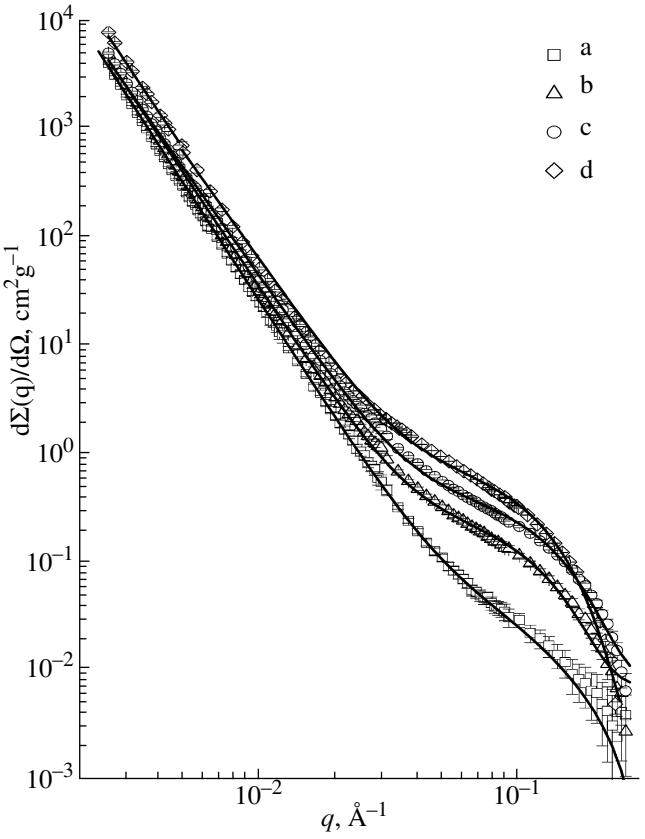

Fig. 2. SANS cross-sections $d\Sigma(q)/d\Omega$ for amorphous $HfO_2 \cdot xH_2O$ xerogels precipitated at pH 4 (a), 6 (b), 8 (c), and 9 (d) vs. momentum transfer q. Continuous lines represent results of experimental data fitting by equation (3).

scattering inhomogeneities are determined by the n value or, more precisely, by the deviation from the Porod asymptotic dependence ($n = 4$) [28]. For volume and mass fractals, n coincides with the fractal dimension D_V, $1 \le D_V \le 3$. For the scattering from three-dimensional objects with fractal surfaces $3 < n = 6 - D_S \le 4$, where D_S is the surface fractal dimension, $2 \le D_S < 3$.

It should be emphasized that a common property for all the samples under study is that two various q ranges exist, where the behaviors of the SANS cross section $d\Sigma(q)/d\Omega$ are significantly different (see Figs. 1 and 2). In particular, for low values $q < q_c$ (where $q_c \approx 0.025$ Å^{-1} is the transition point from one scattering mode to another), the scattering cross section $d\Sigma(q)/d\Omega$ for all the samples satisfies the power law q^{-n}. As it is known, such a power-law dependence is observed for a wide size distribution of scattering inhomogeneities with the relation $R_{max} \gg R_{min}$ if the condition

$$R_{max}^{-1} \ll q \ll R_{min}^{-1} \qquad (2)$$

is satisfied. In addition, the power scattering law means that inhomogeneities making the dominant contribution to scattering are sufficiently large, so that $q_{min}R \gg 1$. Bale and Schmidt [29] proposed a more exact criterion for a certain characteristic size of inhomogeneities, $q_{min}R \approx 3.5$. In our case, $q_{min} = 2 \times 10^{-3}$ Å^{-1} and the characteristic size of the inhomogeneities is equal to $R \approx 1700$ Å.

The exponent n values found from the slope of the straight-line sections of the experimental curves $d\Sigma(q)/d\Omega$ plotted in log–log scale lie in the range from 3.4 to 3.97 for amorphous xerogels of hydrous zirconia and from 3.38 to 3.95 for amorphous xerogels of hydrous hafnia, respectively. As mentioned above, if the exponent value is in the range $3 < n \le 4$, scattering from the samples occurs on the fractal surface with the dimension $2 \le D_S = 6 - n < 3$.

Thus, the further analysis of scattering in the region $q < q_c$ was performed using the two-phase model (solid phase-pore) of the porous material with the fractal surface of the phase interface [28]. According to this model, an object consists of inhomogeneities (pores) with a strongly developed surface, so that, if the total area of the inhomogeneity (pore) surface measured in the scale of the inhomogeneity (pore) surface size R is proportional to R^2, the area of the surface of the scale $r \ll R$ is equal to $R^2(R/r)^D$, where $0 < D < 1$ and $n = 4 - D$. In this case, the fractal dimension of the surface, $D_S = 2 + D$, is larger than two.

Table 1. Parameters of mesostructure of $ZrO_2 \cdot xH_2O$ amorphous xerogels according to SANS and USANS measurements

	Zr-N3	Zr-N4	Zr-N5	Zr-N6	Zr-N7	Zr-N7.5	Zr-N8	Zr-N9
R_g, Å	22700 ± 400	–	21800 ± 450	–	28500 ± 500	–	–	31800 ± 500
$D_S = 6 - \Delta$(USANS)	2.0 ± 0.05	–	2.03 ± 0.05	–	2.29 ± 0.05	–	–	2.62 ± 0.05
$A_1(D_S) \times 10^6$, $cm^{-2}\ g^{-1}$	0.14 ± 0.01	0.1 ± 0.01	0.22 ± 0.01	0.35 ± 0.04	4.1 ± 0.07	3.5 ± 0.06	3.2 ± 0.05	2.01 ± 0.04
$D_S = 6 - n$(SANS)	2.03 ± 0.03	2.03 ± 0.04	2.05 ± 0.04	2.35 ± 0.04	2.3 ± 0.04	2.34 ± 0.04	2.49 ± 0.06	2.6 ± 0.04
$A_2 \times 10^{-1}$, $cm^2\ g^{-1}$	0.21 ± 0.02	0.31 ± 0.02	0.55 ± 0.02	2.6 ± 0.1	4.71 ± 0.02	5.34 ± 0.02	5.58 ± 0.02	7.27 ± 0.02
r_g, Å	13.7 ± 0.8	14 ± 0.7	14.7 ± 0.5	12.9 ± 0.4	15.8 ± 0.4	15.9 ± 0.4	16.1 ± 0.4	16.9 ± 0.4
S_0, $m^2\ g^{-1}$	2 ± 0.4	3 ± 0.5	5 ± 0.5	100 ± 2.5	153 ± 3.5	171 ± 4	189 ± 4	206 ± 4.5

Table 2. Parameters of mesostructure of $HfO_2 \cdot xH_2O$ amorphous xerogels according to SANS and USANS measurements

	Hf-N3	Hf-N4	Hf-N6	Hf-N7	Hf-N8	Hf-N9
R_g, Å	–	14000 ± 200	15100 ± 200	12100 ± 200	12300 ± 500	–
$D_S = 6 - \Delta$(USANS)	–	2.05 ± 0.05	2.15 ± 0.05	2.32 ± 0.05	2.5 ± 0.05	–
$A_1 \times 10^6$, $cm^{-2}\ g^{-1}$	0.4 ± 0.2	2.5 ± 0.5	4.1 ± 1.4	12.3 ± 0.5	52 ± 3	74 ± 20
$D_S = 6 - n$(SANS)	2.05 ± 0.02	2.05 ± 0.04	2.17 ± 0.05	2.35 ± 0.05	2.53 ± 0.04	2.62 ± 0.04
$A_2 \times 10^{-1}$, $cm^2\ g^{-1}$	0.52 ± 0.05	0.57 ± 0.05	2.71 ± 0.06	4.08 ± 0.07	4.32 ± 0.07	5.3 ± 0.08
r_g, Å	17.7 ± 1.1	17.4 ± 0.9	16.2 ± 0.8	14.5 ± 0.8	14.4 ± 0.7	13.6 ± 0.9
S_0, $m^2\ g^{-1}$	3.7 ± 0.2	4.3 ± 0.2	8.4 ± 0.4	27 ± 2	45 ± 3	78 ± 4

In the region $q > q_c$, the scattering curves exhibit a so-called shoulder indicating the presence of small monodisperse inhomogeneities with the effective gyration radius r_g.

Thus, the observed scattering patterns (Figs. 1 and 2) indicates that the xerogels under investigation contain two types of scattering inhomogeneities with strongly different characteristic scales. It can be concluded that $ZrO_2 \cdot xH_2O$ and $HfO_2 \cdot xH_2O$ xerogels are composed of aggregates with a strongly developed surface that are formed from the initial small monomer particles. In the case of xerogels synthesized at pH ≥ 6 phase boundary exhibits fractal behavior.

The power-law dependence of the scattering cross section $d\Sigma(q)/d\Omega$, is usually observed for large q values, whereas the Guinier regime from which an upper estimate can be obtained for the scale of scattering inhomogeneities is observed for small q values. The absence of the Guinier region on the scattering curves for low q values means that the gyration radius R_g or, for the fractal systems, the upper self-similarity boundary is larger than the maximum size R_{max} of the inhomogeneities that can be detected in the experiment with a given resolution. In turn, the lower self-similarity boundary is likely to be determined by the size r_c of the monomer particles, which usually lies in the range from r_g to $1.5r_g$ ($(5/3)^{1/2}r_g$ for spheres) [30].

In view of this circumstance, to analyze scattering from amorphous xerogels of hydrous zirconia and hafnia over the entire q range under investigation, we used the expression [30]:

$$\frac{d\Sigma(q)}{d\Omega} = \frac{A_1(D_S)}{q^n} + A_2\exp\left(-\frac{q^2r_g^2}{3}\right). \quad (3)$$

Here, $A_1(D_S)$ and A_2 are the free parameters, the first of which depends on the system fractal dimension [30] and the second is proportional to the product of the number of monodisperse inhomogeneities in the scattering volume and the neutron scattering amplitude density ρ on them [31].

To obtain the final results, expression (3) was convolved with the setup resolution function. The experimental data for the dependence of the differential cross section $d\Sigma(q)/d\Omega$ were processed by the least mean squares method over the entire q range under investigation. The results of this analysis are given in Figs. 1, 2 and in Tables 1 and 2.

It is well known that for porous materials consisting of two homogeneous phases, parameter $A_1(D_S)$ is related to the phase-interface surface as [30]:

$$A_2(D_S) = \pi\rho^2\Gamma(5 - D_S)\sin[(D_S - 1)(\pi/2)]N_0, \quad (4)$$

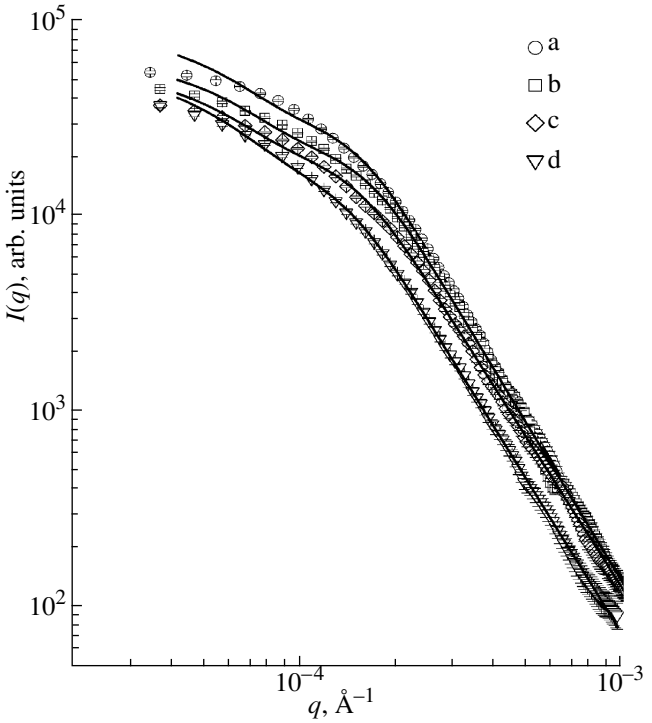

Fig. 3. USANS intensity $I(q)$ for amorphous $ZrO_2 \cdot xH_2O$ xerogels precipitated at pH 3 (a), 5 (b), 7 (c), and 9 (d) vs. momentum transfer q. Continuous lines represent results of experimental data fitting by equation (6).

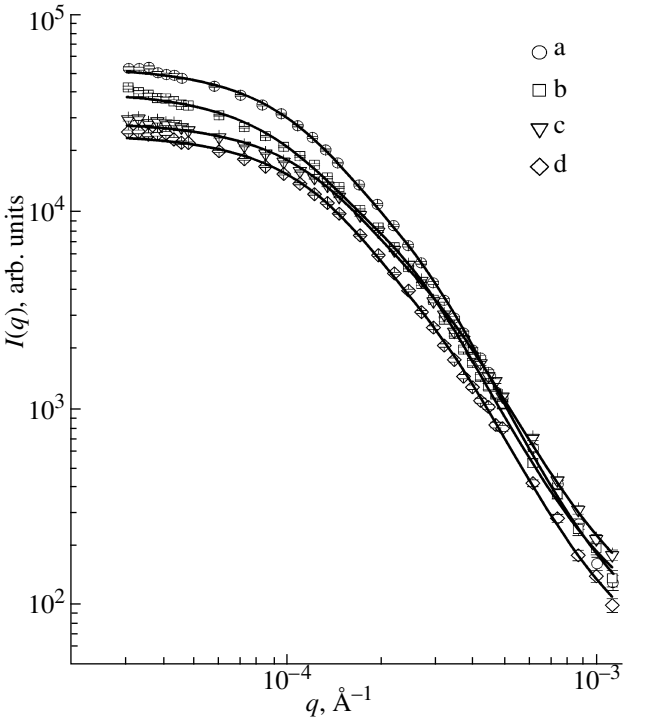

Fig. 4. USANS intensity $I(q)$ for amorphous $HfO_2 \cdot xH_2O$ xerogels precipitated at pH 4 (a), 6 (b), 7 (c), and 8 (d) vs. momentum transfer q. Continuous lines represent results of experimental data fitting by equation (6).

where N_0 is the characteristic of the fractal boundary, Γ is the gamma function, ρ_h is the solid-phase density, and ρ for a molecule containing several elements is defined as:

$$\rho = \sum_i b_i N_i \frac{\rho_h N_A}{M}. \quad (5)$$

Here, N_A is the Avogadro constant, M is the molar mass, b_i is the scattering length for the i-th element in the molecule, and N_i is the number of atoms of this element. The constant N_0 in Eq. (4) is related to the specific surface area (S_0) of the surface fractal as $S_0 = N_0 r^{2-D_S}$, where r^{2-D_S} is determined by the length of the yardstick. For smooth surfaces, $D_S = 2$ and $N_0 = S_0$.

The values of S_0 for both zirconia and hafnia xerogels estimated by standard procedure [32] are given in Tables 1 and 2.

In order to find out self-similarity ranges for the surface fractals obtained we have additionally studied amorphous xerogels of hydrous zirconia and hafnia using USANS technique in a broad range of the momentum transfer. Figures 3 and 4 show the experimental curves of the intensity $I(q)$ of ultra small angle neutron scattering for amorphous xerogels of hydrous zirconia (samples Zr-N3, Zr-N5, Zr-N7 and Zr-N9) and hafnia (samples Hf-N4, Hf-N6, Hf-N7 and Hf-N8). Note that upon increase in the precipitation pH the USANS intensity at $q < 1 \times 10^{-4}$ Å decreases, evidencing the increase in the homogeneity of these xerogels in the nuclear density in the range 1–20 μm.

According to Figs. 3 and 4, for all the samples two different q ranges exist, where the behaviors of the USANS intensity $I(q)$ are significantly different. For $q > 0.0002$ Å^{-1} the scattering intensity $I(q)$ for all the samples satisfies the power law $q^{-\delta}$. The exponent δ values found from the slope of the straight-line parts of the curves plotted in log-log scale (see Figs. 3 and 4) varies from 2.38 to 3 for amorphous xerogels of hydrous zirconia and from 2.5 to 2.95 for amorphous xerogels of hydrous hafnia, respectively.

Deviations from the power law are observed for all the samples at lower values of momentum transfer q (smaller than 0.0002 Å^{-1}). Such deviations are caused by approaching the Guinier regime, where the scattering is determined by the maximum size R_c of independently scattering inhomogeneities. Analysis of the slopes of the curves in Guinier region ($\ln(I(q))$ versus q^2) allows one to evaluate the values of the gyration radii R_g of such inhomogeneities as well as their characteristic size R_c [30]. In turn, upper self-similarity limit is determined as R_c value.

In view of this circumstance, to analyze the scattering from amorphous hydrous zirconia and hafnia xero-

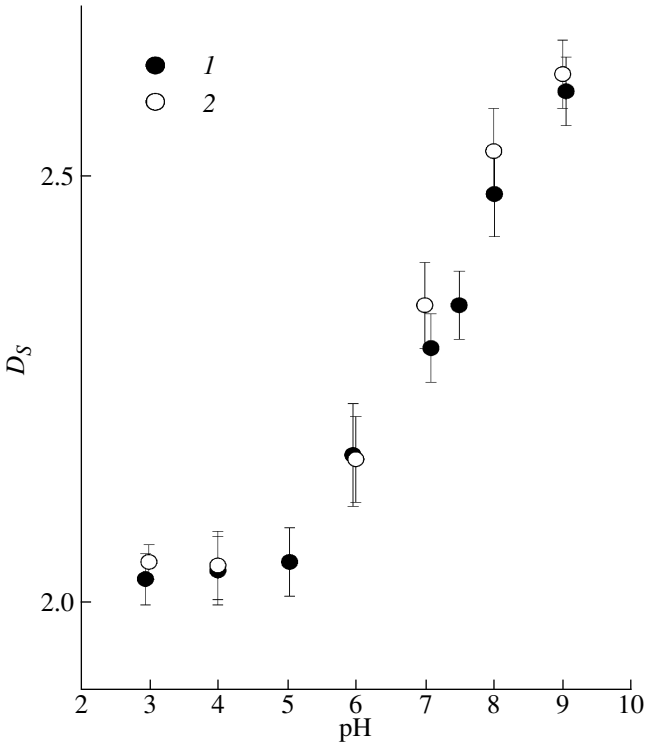

Fig. 5. Surface fractal dimensions D_S of hydrous ZrO_2 (*1*) and HfO_2 (*2*) xerogels precipitated at various pH values.

gels over the entire q range, we used the generalized exponential-power approximation [33]:

$$I(q) = A_3 \exp\left(-\frac{q^2 R_g^2}{3}\right) + \frac{A_4(D_S)}{(\hat{q})^{\delta}}. \qquad (6)$$

Here, $\hat{q} = q/[erf(qR_g/6^{1/2})]^3$ – momentum q transferred, normalized to an error function $erf(x)$. Such a procedure allows the intensity of the scattering $I(q)$ to be described correctly in the intermediate region between $qR_c < 1$ (Guinier approximation) and $qR_c \gg 1$ ($q^{-\delta}$ asymptotics), where scattering from both surfaces and aggregates of characteristic size R_c contributes. Amplitude A_3 is free parameter, which is in direct proportion to the product of number of large aggregates or monodisperse inhomogeneities in scattering volume, respectively, and the density of the neutron scattering amplitude [31]. Amplitude $A_4(D_S)$ depends on the fractal dimension of the system [30]. The $I(q)$ values calculated using Eq. (6) with the parameters determined by the least mean squares method are depicted by solid curves in Figs. 3 and 4.

For the correct comparison of USANS data with the results of the conventional SANS experiments, it was taken into account that the exponent in the dependence of the scattering intensity on the momentum transfer in double-crystal technique measurements is increased by 1 [34]. Therefore, the asymptotic behavior of the intensity of USANS for amorphous xerogels of hydrous zirconia and hafnia in the interval $q \in [0.0002, 0.001]$ Å^{-1} is satisfactorily described by the relation $I(q) \propto q^{-\Delta}$, where $3 < \Delta = \delta + 1 = \leq 4$, that is equivalent to the scattering on a surface fractal with the dimensions $2 \leq D_S = 6 - \Delta < 3$. The values of the fractal dimension D_S obtained from the analysis of the USANS data for amorphous xerogels of hydrous zirconia and hafnia are D_S = 2, 2.03, 2.29 and 2.62 for Zr-N3, Zr-N5, Zr-N7 and Zr-N9 samples and D_S = 2.05, 2.15, 2.32 and 2.5 for Hf-N4, Hf-N6, Hf-N7 and Hf-N8 samples, respectively. These values (with an allowance for measuring accuracy) are very close to the estimates (D_S = 2.03, 2.05, 2.30 and 2.60 for amorphous xerogels of hydrous zirconia and D_S = 2.05, 2.17, 2.35 and 2.53 for amorphous xerogels of hydrous hafnia, respectively) obtained in conventional SANS measurements (Tables 1 and 2).

SANS and USANS data reveal substantial difference between hydrous zirconia xerogels synthesized at low and high pH values. Zr-N3, Zr-N4 and Zr-N5 samples can be considered as non-fractal ($D_S \approx 2$). Increase of precipitation pH up to 6 results in sudden change of the slope of SANS intensity curve as a function of modulus of the scattering angle evidencing formation of surface fractal ($D_S = 2.18 \pm 0.04$). In turn, precipitation of hydrous zirconia at pH 7, 7.5, 8 and 9 leads to the further increase of the surface fractal dimension from 2.30 ± 0.04 to 2.60 ± 0.04 with the increase of pH. Thus we can state that precipitation conditions influence strongly the mesostructure of xerogels and this effect is obviously due to change of colloid particles aggregation mechanism upon change of acidity of the media.

Analysis of SANS and USANS data for hydrous hafnia xerogels reveals the similarity between the structure of these xerogels and hydrous zirconia xerogels. This is expressed in both similar scattering behavior for hafnia and zirconia xerogels (Figs. 1–4) and in similar dependence of scattering intensity from precipitation pH. As in the case of the hydrous zirconia xerogels, the increase of precipitation pH for hydrous hafnia xerogels also results in the transition from non-fractals to surface fractals, and the corresponding dependencies of fractal dimension from precipitation pH are the same (see Fig. 5). However, it should be noted that further analysis performed revealed significant difference in both the size of monomer particles (r_c) and large aggregates (R_c) of hydrous zirconia and hafnia as well as in the dependence of these structural parameters from precipitation pH (see Figs. 6 and 7).

In fact, similarity of the structure of hydrous zirconia and hafnia xerogels is mostly due to the similar chemical properties of zirconium and hafnium. For instance, it was established [35] that the standard thermodynamic characteristics ($\Delta H°$, $\Delta G°$) of Zr and Hf hydroxocomlexes formation upon hydrolysis of metal halides are nearly the same.

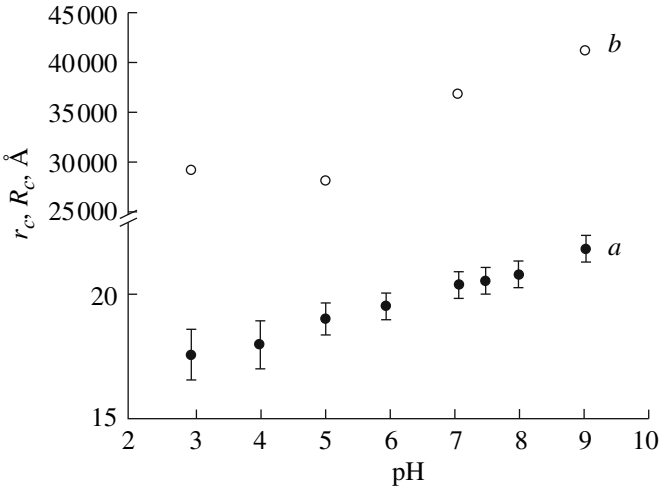

Fig. 6. Maximum monomer r_c (*a*) and aggregate R_c (*b*) sizes for hydrous ZrO_2 xerogels precipitated at various pH.

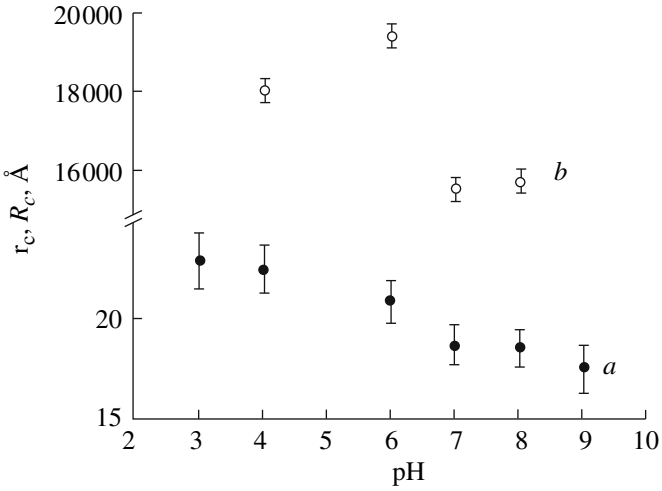

Fig. 7. Maximum monomer r_c (*a*) and aggregate R_c (*b*) sizes for hydrous HfO_2 xerogels precipitated at various pH.

Observed transition between non-fractal aggregates and surface fractals is of especial interest. According to well established models of diffusion limited monomer-cluster and cluster-cluster aggregation, reaction limited aggregation etc., changes in aggregation parameters could result in the change of the fractal dimension. It is also known [36, 37] that in several cases thus formed materials can simultaneously possess surface and mass fractal properties, but these properties appear at different length scales; for example, Liang *et al.* [37] has shown that supercritically dried zirconia alcogels has a typical mass fractal structure constructed by the surface fractal particles. In turn, information on non-fractal to surface fractal transformation upon the change of external conditions is nearly absent. We can conclude that hydrous zirconia and hafnia xerogels can be judged as promising model objects for the further study of peculiarities of such transformation.

Formation of zirconia and hafnia surface fractal aggregates at higher pH values (pH ≥ 6) can be explained using well known data on the mechanism of condensation of hydrous silica monomers [38]. It was established that under acidic conditions condensation occurs mainly between silanol groups located at the ends of polymeric chains leading to the formation of linear polymers. On the other hand, under basic conditions, the condensation reaction will preferentially occur between the ends and the middle of polymeric chains thus leading to formation of more ramified aggregates with a larger fractal dimension. Such an approach can be successfully used to explain the increase of surface fractal dimension value of hydrous zirconia upon gradual increase of precipitation pH from 6 to 9. These suppositions are also in agreement with well established Clearfield theory [39], which states that slow hydrolysis of zirconyl salts leads to formation of regular sheets consisting of tetrameric $Zr_4(OH)_8$ units, while fast hydrolysis (for instance, under basic conditions) promotes rapid polymerization occurring in many directions at once. It should be also noted that, according to [40], the degree of polymerization increases with an increase of pH. We can assume that such a mechanism of polymerization can be the main reason of fractal formation in course of hydrous zirconia oxide precipitation. In such a way, we can also suppose that further increase of pH will result in formation of hydrous zirconia samples with even higher surface fractal dimension.

SANS data indicate that the size of primary particles formed during hydrolysis of both $ZrO(NO_3)_2$ and $HfCl_4$ depends on the precipitation conditions. Increase of precipitation pH leads to monotonous increase of the size of hydrous zirconia particles from 13.7 ± 0.8 Å to 16.9 ± 0.4 Å, while for hafnia particles the opposite tendency is observed: the particle size decreases from 17.7 ± 1.1 Å to 13.6 ± 0.9 Å [41, 42]. The exact nature of such a phenomenon is to be further clarified. However, one should note that the particle size determined by SANS corresponds well to size of crystallites (~10 Å) with short-range ordering determined by synchrotron diffraction study [18].

Low temperature nitrogen adsorption measurements give additional information on the mesostructure of zirconia xerogels. Measurements of specific surface area of hydrous zirconia samples were performed by low temperature nitrogen adsorption using QuantaChrome Nova 4200B analyzer. Before measurements the samples were outgased at 40°C for 5 h in vacuum. Determination of the surface area was carried out by Brunauer–Emmett–Teller (BET) method using 28 points. Analysis of pore size distribution was performed on the basis of nitrogen desorption isotherms using Barret–Joyner–Halenda (BJH) method.

According to multi-point BET data, one can see a notable difference between samples prepared under

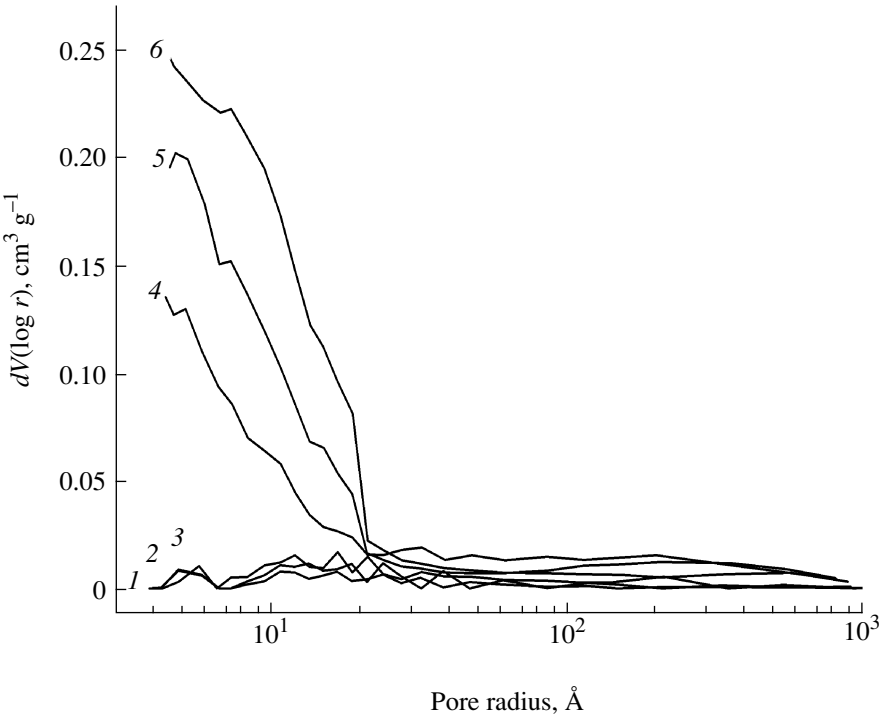

Fig. 8. BJH pore size distributions for zirconia xerogels Zr-N3 (*1*); Zr-N4 (*2*); Zr-N5 (*3*); Zr-N6 (*4*); Zr-N7 (*5*); Zr-N9 (*6*).

acidic conditions (up to pH 5) and neutral and slightly alkaline conditions (pH 6 and higher). Each of xerogels belonging to the first group possesses extremely low specific surface area (2 ± 2, 3 ± 2 and 2 ± 2 m^2/g for Zr-N3, Zr-N4 and Zr-N5, respectively), which in fact cannot be measured with enough precision. At higher pH values specific surface area raises tremendously up to 100 ± 5, 185 ± 5 and 236 ± 5 m^2/g for Zr-N6, Zr-N7 and Zr-N9, respectively. The results presented coinside with the data presented in [41, 43, 44]. Analysis of nitrogen adsorption data using BJH method verifies BET data. Samples Zr-N3, Zr-N4 and Zr-N5 can be judged as virtually non-porous (pore volume is less than 0.01 cm^3/g), while samples Zr-N6, Zr-N7 and Zr-N9 are microporous (mean pore sizes are 2.0, 4.6 and 4.6 Å, specific pore volumes are 0.04 ± 0.01, 0.09 ± 0.01 and 0.13 ± 0.01 cm^3/g, respectively). BJH pore size distributions for samples of zirconia xerogels are shown in Fig. 8.

Results of low temperature nitrogen adsorption measurements are in a good agreement with the model of hydrous zirconia polymerization and aggregation described above. In fact, xerogel samples precipitated at low pH values possess low specific surface area and are nearly non-porous. In other words, they can be judged as dense aggregates consisting of monomer particles which packing is compact (non-fractal). Increase of precipitation pH up to pH_{pzc} and higher results in loose packing of monomers and formation of ramified aggregates possessing well-developed surface and containing sufficiently large amount of micropores. It should be noted that observed increase of porosity corresponds well with previously reported data on the influence of precipitation pH on the apparent density of hydrous zirconia gels [45, 46]. For instance, it was established [46] that the densities of hydrogels precipitated at pH 6, 8 and 9 are equal to 3.52, 3.21 and 3.04 g cm^{-3}, respectively. The same changes of apparent density upon the increase of precipitation pH are also observed for the samples Zr-N3, Zr-N5, Zr-N6, Zr-N7, Zr-N8 and Zr-N9.

III. THERMAL DECOMPOSITION OF HYDROUS ZIRCONIA AND HAFNIA

Thermogravimetric and differential thermal (TGA/DTA) analysis of hydrous zirconia xerogels was performed using Pyris Diamond thermoanalyzer (Perkin–Elmer) in the temperature range 20–1000°C at a heating rate of 10°C/min in air.

Figure 9 shows TG curves of samples Zr-N3, Zr-N6 and Zr-N9. One can see that there is a noticeable difference in thermal behavior of samples precipitated at low (pH 3–5) and high (pH 6–9) pH values. TG/DTA curves of Zr-N3, Zr-N4, Zr-N5 indicate that decomposition of these samples proceeds in two stages up to 415°C where abrupt mass loss accompanied by sharp exothermic peak is observed.

In turn, the decomposition of Zr-N6, Zr-N7 and Zr-N9 proceeds in the same way but without dramatic mass loss above 400°C. It should be noted that the exothermic peak is also found in DTA curves of these sam-

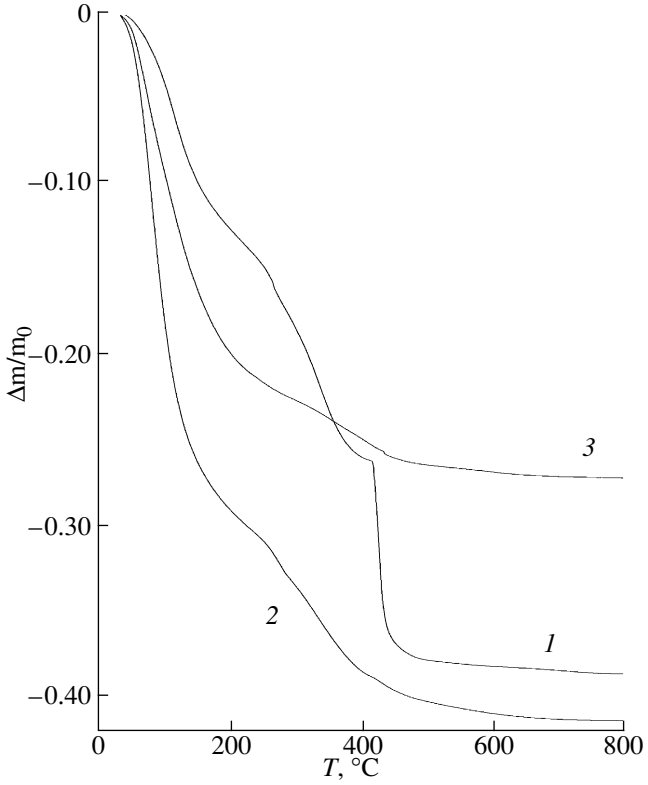

Fig. 9. Results of thermal analysis of zirconia xerogels Zr-N3 (*1*), Zr-N6 (*2*), Zr-N9 (*3*).

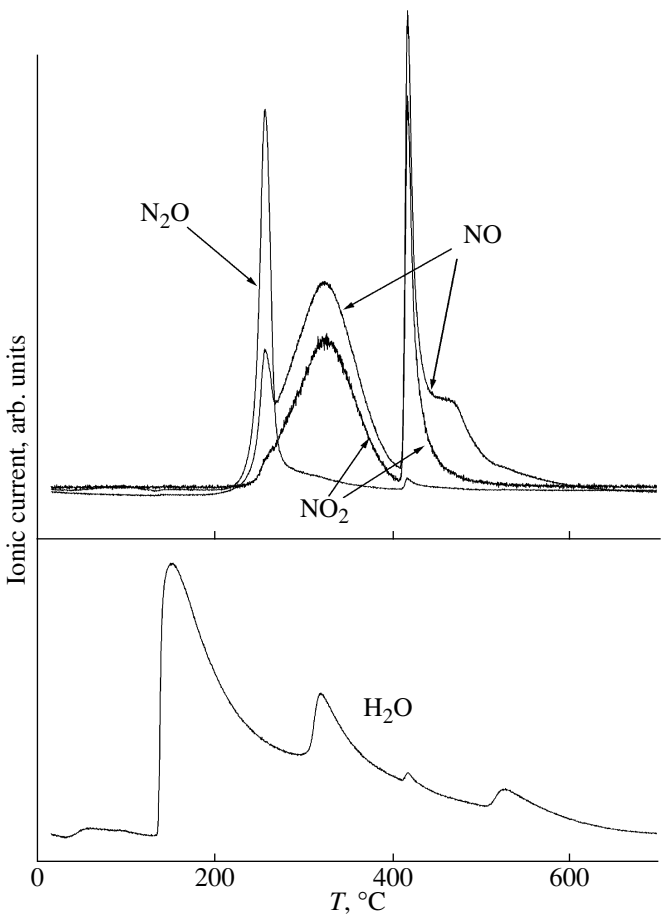

Fig. 10. Results of thermal analysis and composition of gases evolved during thermal decomposition of Zr-N5 sample.

ples but it is slightly shifted toward higher temperatures (426–435°C).

Thermal analysis and mass spectrometry of gases evolved (TGA/MS) were carried out using TG 209F1 Iris analyzer (Netzch) coupled with QMS 403C Aeolos mass spectrometer (Netzch) at a heating rate of 10°C/min in argon. TGA/MS data indicate (Fig. 10) that thermal decomposition of the samples under study exhibit rather complex behavior. At relatively low temperatures (up to ~200–250°C), substantial mass loss is mainly due to removal of water. Upon heating up to ~260°C evolving of N_2O (CO_2) is detected accompanied with slight increase of the decomposition rate. Mass loss at 300–400°C is caused by evolving of NO, NO_2 and water. Finally, abrupt mass loss at 410–430°C observed for samples prepared at lower pH values (below pH 5) is also accompanied by evolving of NO/NO_2. Semi-quantitative analysis of MS data allows to state that total nitrogen content in xerogels prepared at lower pH values (Zr-N3, Zr-N4, Zr-N5) is about 2.5–8 times higher than the nitrogen content in xerogels prepared at higher pH values (Zr-N6, Zr-N7, Zr-N9).

Analysis of TGA/DTA/MS data indicates that conditions of hydrous zirconia precipitation affect substantially the subsequent thermal behavior of the samples. The main difference between the samples precipitated at lower pH values ($pH < pH_{pzc}$) and the samples precipitated at higher pH values ($pH \geq pH_{pzc}$) is in the content of bound nitrogen. The amount of N_2O (CO_2), NO and NO_2 evolving during annealing of xerogels is decreased upon increase of precipitation pH. These results confirm the fact that adsorption of NO_3^- and NH_4^+ ions onto the surface of hydrous zirconia gels obtained at pH_{pzc} and above this point is significantly less pronounced. Similar results were obtained in [43, 44] during the study of hydrous zirconia samples prepared from zirconium oxynitrate and zirconium oxychloride. It was demonstrated that the gels precipitated at $pH \leq 6$ mostly contain sorbate nitrate ions and those precipitated at $pH \geq 7$ mostly contain sorbate ammonium ions. TGA/DTA/MS data allow also to explain the origin of mass loss at 415–435°C accompanied by sharp exothermic peak. Obviously, these effects are caused by rapid exothermal crystallization of zirconium dioxide [47] and simultaneous decomposition of

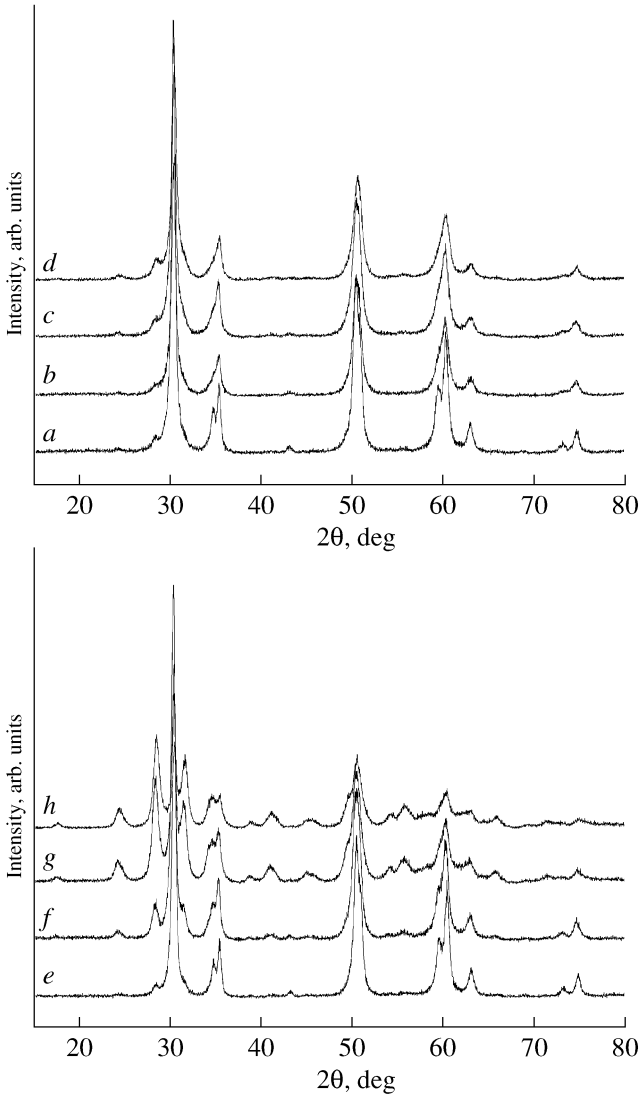

Fig. 11. X-ray diffraction patterns of *a*—Zr-N3-500, *b*—Zr-N6-500, *c*—Zr-N7-500, *d*—Zr-N9-500, *e*—Zr-N3-600, *f*—Zr-N6-600, *g*—Zr-N7-600, and *h*—Zr-N9-600.

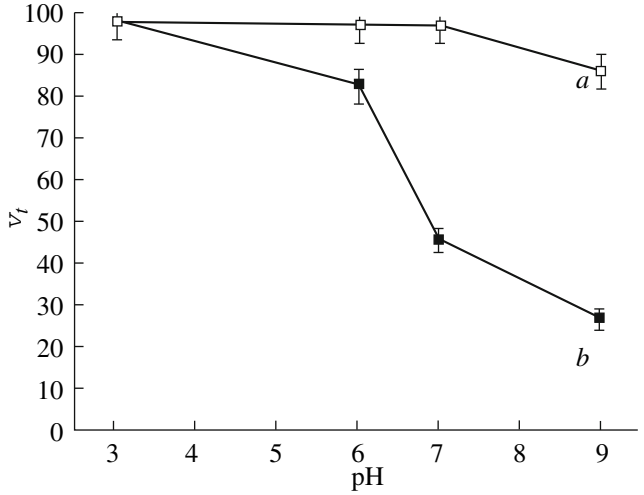

Fig. 12. Volume fractions of tetragonal ZrO_2 in samples annealed at *a*—500°C and *b*—600°C.

residual nitrates with NO/NO_2 emission. We can further assert that interpretation of nearly analogous data [48], based on assumption that precipitation at low pH values results in formation of new zirconium hydroxide ($Zr_4O_3(OH)_{10} \cdot 6H_2O$), is probably incorrect.

As it was mentioned above, annealing of zirconia xerogels at 270°C for 5 hours did not result in formation of crystalline phases. After treatment at higher temperature (380°C) all the samples give practically identical diffractograms which are typical for pure metastable tetragonal ZrO_2 modification. Nevertheless, very weak peak (~24°2θ) corresponding to merged (110) and (011) reflections of monoclinic ZrO_2 can be observed at XRD pattern of Zr-N9-380.

Figure 11 represents XRD data for all zirconia samples, obtained at 500 and 600°C. One can see that variation of precipitation conditions strongly affects the phase composition of annealed products. Obviously, thermal treatment of samples synthesized at higher precipitation pH results in an increase of content of stable monoclinic zirconia in the reaction mixtures.

Volume fractions of monoclinic (m-ZrO_2) and tetragonal (t-ZrO_2) phases in zirconia samples (x_m and x_t, respectively) were estimated using equations proposed by Toraya [49]:

$$x = \frac{I_m(\bar{1}11) + I_m(111)}{I_m(\bar{1}11) + I_m(111) + I_t(111)}, \quad (7)$$

$$v_m = \frac{1.311x}{1 + 0.311x}, \quad (8)$$

$$v_t = 1 - v_m, \quad (9)$$

where $I_m(\bar{1}11)$, $I_m(111)$ are the integral intensities of ($\bar{1}11$) and (111) m-ZrO_2 diffraction maxima, $I_t(111)$ is the integral intensity of (111) t-ZrO_2 diffraction maximum, v_m and v_t are volume fractions of monoclinic and tetragonal zirconia in the mixture, respectively.

Thus calculated volume fractions of tetragonal zirconia in annealed samples are presented in Fig. 12.

Formation of crystalline zirconia at 380°C, i.e. at the temperature considerably below the position of exothermic peaks in the DTA curves, is in a good agreement with the data obtained by Glushkova *et al.* [50]. However the difference in particle sizes for the powders annealed at low (380°C) and high (500–600°C) temper-

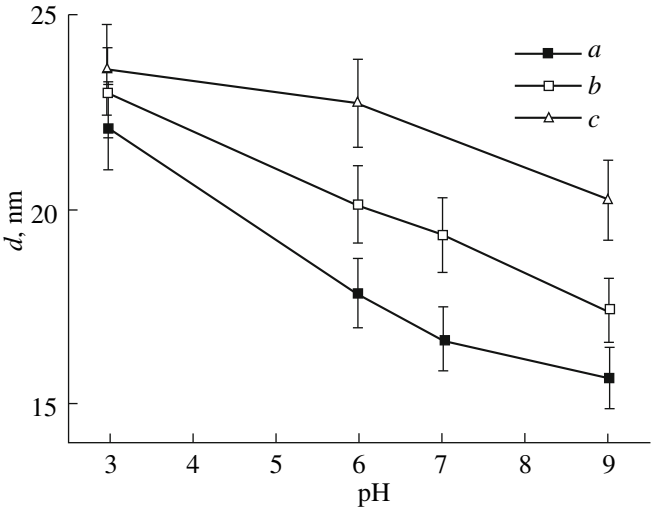

Fig. 13. Particle size of tetragonal zirconia upon annealing of xerogels at *a*—380°C, *b*—500°C, and *c*—600°C.

atures is not as large as reported in [50]. According to [17, 51], transition of metastable tetragonal to a stable monoclinic ZrO_2 phase is hindered by defects. In particular, it was found [17] that thermal treatment of samples containing a large number of NO_3-groups results in preferential formation of tetragonal zirconia. Our data indicate that such an effect actually takes place and tetragonal to monoclinic phase transition occurs faster for the samples of hydrous zirconia precipitated at higher pH values (>6). In turn, annealing of hydrous zirconia samples obtained at low pH values (i.e. pH ~ 3) results in formation of pure tetragonal ZrO_2 due to large amount of residual NO_3-groups sorbed and incorporated into the structure of gel upon precipitation at $pH < pH_{pzc}$.

Mean particle size for zirconia samples after thermal treatment were calculated using Scherer equation:

$$D_{hkl} = \frac{K\lambda}{\beta_{hkl}(2\theta)\cos(\theta_0)}, \quad (10)$$

where θ_0—position of peak maximum, λ—wavelength of CuK_α radiation (0.154056 nm), $\beta_{hkl}(2\theta)$—true width at half height of diffraction maximum. The value of Scherrer constant (K) was taken to be equal to 1.

True width on half height of diffraction was calculated as follows:

$$\beta_{hkl} = \beta - s, \quad (11)$$

where β—full width on half height of maximum, s—instrumental broadening (0.09 ± 0.01° 2θ). Contribution of microstrains into diffracton peak broadening was not taken into account. Instrumental broadening was established using standard sample of monocrystalline sapphire.

Full width on half height of diffraction maximum value (β) was calculated as follows. After subtraction of the baseline diffraction lines (101) for t-ZrO_2, ($\bar{1}11$) and (111) for m-ZrO_2 and m-HfO_2 in the range 20°–40° 2θ were described by pseudo-Voigt function

$$V(\theta) = \frac{2cA}{\pi}\left[\frac{\omega_L}{4(\theta-\theta_0)^2+\omega_L^2}\right] + \frac{2(1-c)A}{\omega_G} \times \sqrt{\frac{\ln 2}{\pi}}\exp\left[-\frac{4\ln 2(\theta-\theta_0)^2}{\omega_G^2}\right], \quad (12)$$

where ω_L, ω_G—lorenzian and gaussian parameters, respectively ($\omega_L = \omega_G = \beta$), A—normalizing factor, c—relative contribution of Lorenz function into overall intensity of the maximum.

XRD data indicates that mean particle size for the samples obtained by thermal decomposition of xerogels synthesized at various pH also depends on precipitation conditions. In fact data presented on Fig. 13 clearly indicate that particle size of tetragonal zirconia obtained upon thermal treatment of xerogels precipitated at low pH values is notably higher compared with particle size of t-ZrO_2 synthesized in neutral and alkaline media. Moreover the decrease or particle size with the increase of pH value can be observed both at low (380°C) and relatively high (500–600°C) annealing temperatures.

It is well known that thermal decomposition of hydrous zirconia can be judged as a topochemical process. In such a way, structure of initial xerogel should affect the structure and properties of the product of its thermal decomposition. It can be concluded that the difference in particle size in t-ZrO_2 synthesized from acidic and alkaline media is governed by the difference in the composition and mesostructure of xerogels. In particular, denser xerogels precipitated at low pH values transform into larger ZrO_2 particles while xerogels possessing more ramified structure decompose upon annealing with formation of relatively small ZrO_2 particles.

It should be also noted that the particle size for stable monoclinic ZrO_2 forming at relatively high temperatures (600°C) also depends upon precipitation pH value. Particle size of m-ZrO_2 in Zr-N7-600 and Zr-N9-600 samples is about 13–14 nm, while in Zr-N6-600 it is significantly higher and is equal to 19–20 nm.

Specific surface area data for zirconia samples synthesized by thermal treatment are in a good agreement

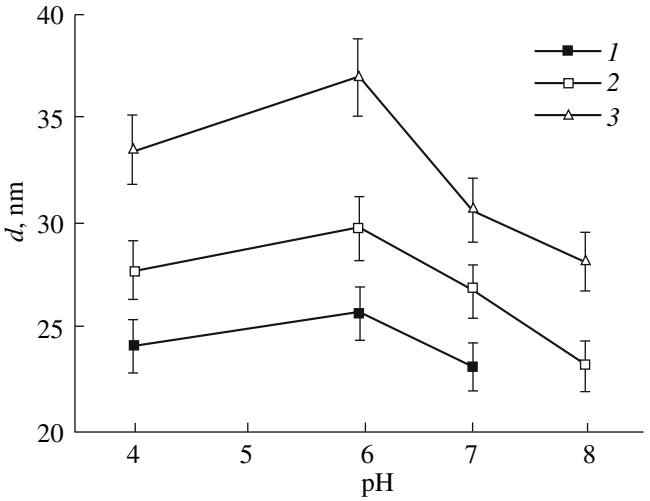

Fig. 14. Particle size of monoclinic hafnia upon annealing of xerogels at *1* – 500°C, *2* – 600°C, and *3* – 700°C.

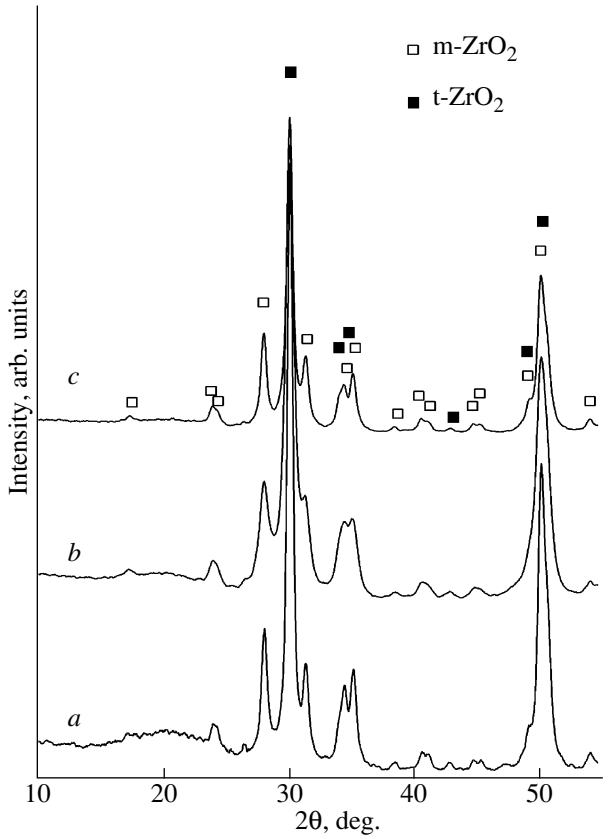

Fig. 15. XRD patterns of hydrous zirconia samples treated hydrothermally at 225°C for 5 hours, *a* – Zr-N4-H, *b* – Zr-N6-H, and *c* – Zr-N7-H.

with the similar results obtained for initial amorphous zirconia xerogels. Actually specific surface area (S_{BET}) of Zr-N3-380 is very low and equal to 8 ± 2 m^2/g (S_{BET}(Zr-N3) ≈ 2 m^2/g). At the same time increase of the precipitation pH up to the point of zero charge and higher leads to dramatic increase of S_{BET} values for corresponding annealed samples. Specific surface areas of Zr-N6-380, Zr-N7-380, Zr-N9-380 samples were found to be 103 ± 10 m^2/g, 130 ± 12 m^2/g and 130 ± 12 m^2/g, respectively. These data give an additional evidence that the microstructure of crystalline zirconia which is formed by annealing of $ZrO_2 \cdot xH_2O$ xerogels is greatly affected by mesostructure of amorphous hydrous zirconia. The same tendency is observed for the samples annealed at higher temperatures (500–600°C). Although S_{BET} values decrease notably with the increase of annealing temperature, the effect mentioned above can be clearly seen. For instance, S_{BET} values for Zr-N3-500 and Zr-N3-600 are the lowest in the series of samples and do not exceed 10 m^2/g. S_{BET} values for Zr-N6-500 and Zr-N6-600 are equal to 73 ± 7 and 37 ± 3 m^2/g, respectively. Specific surface areas for Zr-N7-500, Zr-N7-600, Zr-N9-500 and Zr-N9-600 samples were found to be 72 ± 7 m^2/g, 49 ± 4 m^2/g, 72 ± 7 m^2/g, and 52 ± 5 m^2/g respectively. Thus the highest surface area of zirconia can be reached when starting hydrous zirconia is precipitated under alkaline conditions (pH > pH_{pzc}).

Thermal treatment of hydrous hafnium dioxide results in direct formation of stable monoclinic HfO_2 phase while metastable tetragonal hafnia doesn't exist. Indeed, our data are in a good agreement with this fact: annealing of hydrous hafnia xerogels at 500–700°C resulted in formation of pure m-HfO_2. At the same time, thermolysis of hydrous hafnia can also be considered as topochemical process, so mesostructure of starting amorphous xerogels also affects the microstructure of resulting crystalline products. Figure 14 presents relation between mean particle size of samples obtained by thermal decomposition of hafnia xerogels at various temperatures (500–700°C).

It should be noted that particle size of m-HfO_2 only slightly depends on starting hydrous hafnia precipitation pH. The overall dependence of particle size versus pH for m-HfO_2 is nearly the same as for t-ZrO_2, while structural differences in samples obtained in acidic and alkaline media are notably lesser. According to low temperature nitrogen adsorption data, HfO_2 powders prepared from xerogels precipitated at low pH values possess lower specific surface. For instance, specific surface areas of Hf-N4-500, Hf-N6-500, Hf-N7-500 and Hf-N8-500 samples were found to be 13 ± 2 m^2/g, 16 ± 2 m^2/g, 23 ± 2 m^2/g, and 24 ± 2 m^2/g, respectively. Upon annealing at higher temperatures (600 and 700°C) the difference in specific surface areas for the samples precipitated at various pH values becomes less significant.

To further clarify peculiarities of nanocrystalline zirconia formation upon decomposition of hydrous zir-

Table 3. Phase composition and mean particle size of zirconia powders synthesized hydrothermally from amorphous $ZrO_2 \cdot xH_2O$ xerogels

Sample	Phase composition	Particle size of t-ZrO_2, nm	Particle size of m-ZrO_2, nm	
			calculated using ($\bar{1}11$) diffraction maximum	calculated using (111) diffraction maximum
Zr-N4-H	0.24% ± 0.02% m-ZrO_2, 0.76% ± 0.02% t-ZrO_2	22 ± 2	22 ± 2	25 ± 2
Zr-N6-H	0.23% ± 0.02% m-ZrO_2, 0.77% ± 0.02% t-ZrO_2	12 ± 2	13 ± 2	15 ± 2
Zr-N7-H	0.32% ± 0.02% m-ZrO_2, 0.68% ± 0.02% t-ZrO_2	20 ± 2	22 ± 2	21 ± 2

conia xerogels several samples of these materials were treated hydrothermally. To do so, aqueous suspensions of zirconia xerogels (100 mg of $ZrO_2 \cdot xH_2O$ in 80 ml of H_2O) were placed into stainless steel autoclave (Parr 4593 equipped with Parr 4836 controller), heated up to 225°C at a heating rate of 5°C/min and then held at this temperature for 5 h. The temperature inside the autoclave was monitored using internal thermocouple. Hydrothermally prepared samples were named Zr-N4-H, Zr-N6-H and Zr-N7-H, respectively.

Figure 15 shows XRD patterns of hydrous zirconia samples treated hydrothermally at 225°C for 5 h. Note that in contrast to xerogels annealed at low temperatures (380°C), these samples consist not only of tetragonal but also of monoclinic modification of zirconia. Table 3 groups some data on phase composition and structural parameters of samples Zr-N4-H, Zr-N6-H and Zr-N7-H.

Figure 16 shows TEM images of Zr-HT6, Zr-T6, Zr-HT7 and Zr-T7 samples taken using Leo912 AB Omega transmission electron microscope (TEM) operating at 100 kV. According to these data, Ostwald ripening takes place both upon annealing and hydrothermal treatment resulting in formation of polydisperse nanopowders. Individual ZrO_2 nanoparticles are strongly aggregated forming self-similar fractal-like clusters of different sizes. Due to polydisperse nature of the powders it is impossible to estimate mean particle size, so such information was obtained solely from the XRD data.

One can see that mean particle size is lowest for Zr-N6-H sample (Table 3). This effect can be due to the fact that starting xerogel (Zr-N6) was precipitated at pH close to the point of zero charge and so contained minimal amount of adsorbed nitrate and ammonium ions. Thus subsequent hydrothermal treatment of the sample has proceeded virtually in the absence of foreign substances and ions (so called mineralizers) which usually greatly increase the rate of dissolution-precipitation processes. In turn, precipitation of hydrous zirconia at lower or higher pH values results in stronger adsorption of ions and therefore facilitates notable crystallite growth under hydrothermal conditions. It should be also noted that even slight increase in precipitation pH (from 6 to 7) facilitates transition of metastable tetragonal zirconia into stable monoclinic modification during subsequent hydrothermal treatment.

IV. CONCLUSIONS

Analysis of SANS and USANS data clearly indicates that hydrous zirconia and hafnia xerogels can be judged as unique objects possessing fractal properties in a wide range of scales. Moreover, the fractal dimension of these xerogels can be finely tuned simply by varying their synthesis conditions, for instance, precipitation pH. It was demonstrated for the first time that mesostructure (including fractal structure and porosity) of hydrous zirconia and hafnia xerogels changes dramatically upon the increase of precipitation pH over the point of zero charge ($pH_{pzc} \approx 6$). It was shown that such an effect is connected with the changes in the adsorption of anions (i.e. NO_3^- and Cl^-) onto the surface of gels. Due to the similarity of zirconium and hafnium chemical properties surface fractal dimensions of hydrous zirconia and hafnia xerogels obtained by precipitation at the same pH values coinside. Finally, it was demonstrated that mean particle size and specific surface area of ZrO_2 and HfO_2 nanopowders depends

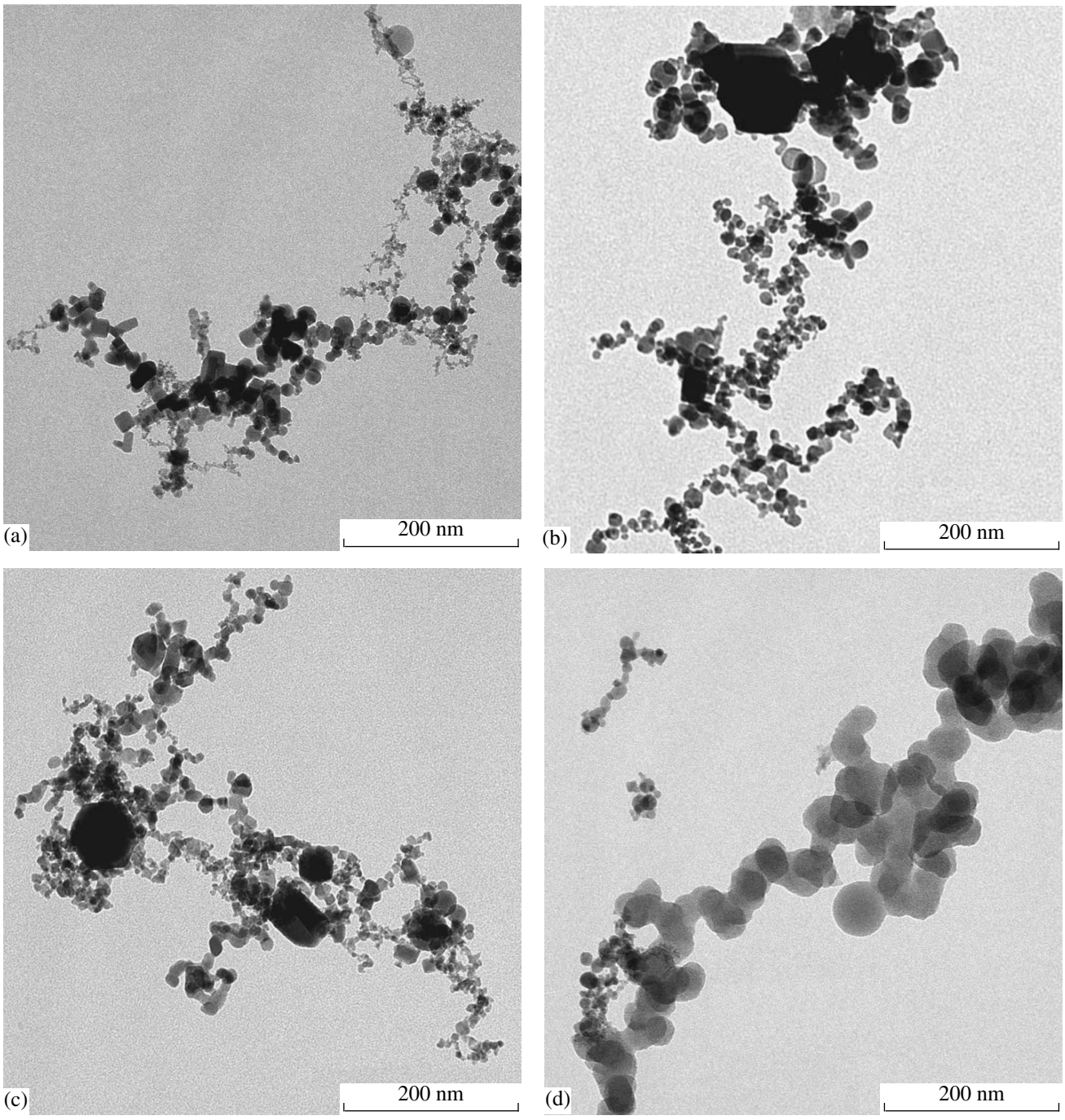

Fig. 16. TEM images of zirconium dioxide (a) Zr-N6-H, (b) Zr-N6-500, (c) Zr-N7-H, and (d) Zr-N7-500.

strongly on the mesostructure and precipitation pH of hydrous zirconia and hafnia xerogels.

ACKNOWLEDGMENTS

This work was supported by RFBR 09-03-12191-ofi-m and 07-02-00290-a grants. V.I., G.K., A.B. and S.G. would like to thank GKSS Forschungszentrum for hearty welcome.

REFERENCES

1. *Binary Rare Earth Oxides*, Ed. by G. Adachi, N. Imanaka, Z. C. Kang (Kluwer, Dordrecht, 2004).
2. G. G. Volkova, S. I. Reshetnikov, L. N. Shkuratova, A. A. Budneva, and E. A. Paukshtis, Chem. Eng. J. **134**, 106 (2007).
3. L. Kaluža and M. Zdražil, Appl. Catal. A **329**, 58 (2007).
4. K. M. Parida and S. Mallick, J. Mol. Catal. A **275**, 77 (2007).

5. I. Matsukuma, S. Kikuyama, R. Kikuchi, K. Sasaki, and K. Eguchi, Appl. Catal. B **37**, 107 (2002).
6. A. Emmerling and J. Fricke, J. Non-Cryst. Solids **145**, 113 (1992).
7. D. R. Vollet, D. A. Donatti, R. A. Ibanez, and H. Macetti, Phys. Rev. B: Condens. Matter **69**, 094203–1 (2004).
8. A. Singhal, L.M. Toth, G. Beaucage, J.-S. Lin, and J. Peterson, J. Coll. Int. Sci. **194**, 470 (1997).
9. O. Stachs and T. Gerber, J. Sol-Gel Sci. Tech. **15**, 23 (1999).
10. Y. W. Zeng, P. Riello, A. Benedetti, and G. Fagherazzi, J. Non-Cryst. Solids **185**, 78 (1995).
11. A. Lecomte, F. Blanchard, A. Dauger, M. C. Silva, and R. Guinebretiere, J. Non-Cryst. Solids **225**, 120 (1998).
12. L. Liang, Y. Xu, X. Hou, D. Wu, Y. Sun, Z. Li, and Z. Wu, J. Solid State Chem. **179**, 959 (2006).
13. C. V. Santilli, S. H. Pulcinelli, and A. F. Craievich, Phys. Rev. B: Condens. Matter **51**, 8801 (1995).
14. M. C. Silva, G. Trolliard, O. Masson, R. Guinebretiere, A. Dauger, A. Lecomte, and B. Frit, J. Sol-Gel Sci. Tech. **8**, 419 (1997).
15. A. C. Geiculescu and H. J. Rack, J. Non-Cryst. Solids **306**, 30 (2002).
16. P. D. Southon, J. R. Bartlett, J. L. Woolfrey, and B. Ben-Nissan, Chem. Mater. 14, 4313 (2002).
17. D. A. Zyuzin, E. M. Moroz, A. S. Ivanova, A. N. Shmakov, and G. N. Kustova, Kinet. Catal. **45**, 739 (2004).
18. D. A. Zyuzin, E. M. Moroz, A. S. Ivanova, and A. N. Shmakov, Crystallogr. Repts. **48**, 413 (2003).
19. A. S. Ivanova, M. A. Fedotov, G. S. Litvak, and E. M. Moroz, Inorg. Mater. **36**, 352 (2000).
20. M. Kosmulski, Coll. Surf. A **222**, 113 (2003).
21. S. I. Pechenyuk, Russ. Chem. Bull. **48**, 1017 (1999).
22. G. A. Parks, Chem. Rev. **65**, 177 (1965).
23. M. Kosmulski, J. Gustafsson, and J. B. Rosenholm, J. Coll. Int. Sci. **209**, 200 (1999).
24. J.-P. Hsu and A. Nacu, J. Coll. Int. Sci. **274**, 277 (2004).
25. G. D. Wignall and F. S. Bates, J. Appl. Cryst. **20**, 28 (1986).
26. W. Schmatz, T. Springer, J. Schelten, and K. Ibel, J. Appl. Crystallogr. **7**, 96 (1974).
27. D. Bellmann, M. Klatt, R. Kampmann, and R. Wagner, Physica B **241–243**, 71 (1998).
28. J. Teixera, *On Growth and Form-Fractal and Non-Fractal Pattern in Physics*, Ed. by H. E. Stanley, N. Ostrovsky (Martinus Nijloff, Boston, 1986).
29. H. D. Bale and P. W. Schmidt, Phys. Rev. Lett. **38**, 596 (1984).
30. P. W. Schmidt, *Modern Aspects of Small-Angle Scattering*, Ed. by H. Brumberger (Kluwer, Dordrecht, 1995).
31. A. Guinier, G. Frournet, C.B. Walker, and K. L. Yudowitch, *Small-Angle Scattering of X-rays* (Wiley, New York/London, 1955).
32. P. Wong and A. J. Bray, Phys. Rev. Lett. **60**, 1344 (1988).
33. G. Beaucage, J. Appl. Crystallogr. **28**, 717 (1995).
34. Yu. G. Abov, D. S. Denisov, N. O. Elyutin, S. K. Matveev, Yu. I. Smirnov, A. O. Eidlin, F. S. Dzheparov, and D. V. L'vov, J. Exper. Theor. Phys. **87**, 1195 (1998).
35. V. P. Vasil'ev, A. I. Lytkin, and N. V. Chernyavskaya, J. Therm. Anal. Calorim. **55**, 1003 (1999).
36. W. G. Rotschild, *Fractals in Chemistry* (Wiley, New York, 1998).
37. L. Liang, Y. Xu, X. Hou, D. Wu, Y. Sun, Z. Li, and Z. Wu, J. Solid State Chem. **179**, 959 (2006).
38. C. J. Brinker, K. D. Keefer, D. W. Schaeffer, R. A. Q. Assink, B. D. Kay, and C. S. Ashley, J. Non-Cryst. Solids **63**, 45 (1984).
39. A. Clearfield, J. Mater. Res. **5**, 161 (1990).
40. T. G. Kuznetsova and V. A. Sadykov, Kinet. Catal. **49**, 840 (2008).
41. G. P. Kopitsa, V. K. Ivanov, S. V. Grigoriev, P. E. Meskin, O. S. Polezhaeva, and V. M. Garamus, JETP Lett. **85**, 122 (2007).
42. V. K. Ivanov, G. P. Kopitsa, A. E. Baranchikov, M. Sharp, and Yu. D. Tret'yakov, Dokl. Chem. **427**, 160 (2009).
43. I. A. Stenina, E. Yu. Voropaeva, A. G. Veresov, G. I. Kapustin, and A. B. Yaroslavtsev, Russ. J. Inorg. Chem. **53**, 350 (2008).
44. I. A. Stenina, E. Yu. Voropaeva, T. R. Brueva, A. A. Sinel'nikov, N. A. Drozdova, V. M. Ievlev, and A. B. Yaroslavtsev, Russ. J. Inorg. Chem. **53**, 842 (2008).
45. S. I. Pechenyuk, Yu. V. Ivanov, and Yu. P. Semushina, Russ. J. Inorg. Chem. **51**, 189 (2006).
46. S. I. Pechenyuk, D. P. Domonov, and V. N. Nakonechnyi, Russ. Chem. Bull. Int. Ed. **54**, 1111 (2005).
47. T. Sato, J. Therm. Anal. Calorim. **69**, 255 (2002).
48. G.-Y. Guo, Y.-L. Chen, and W.-J. Ying, Mat. Chem. Phys. 84, 308 (2004).
49. H. Toraya, M. Yoshimura, and S. Somiya, Comm. Am. Ceram. Soc. **67**, C—119 (1984).
50. V. B. Glushkova and A. N. Lapshin, Glass Phys. Chem. **29**, 415 (2003).
51. M. I. Domnina and S. K. Filatov, Neorg. Mater. **19**, 920 (1983).